Response to reviewer #2

Item-by-item responses to the specific comments are provided below, in which the reviews' comments are in **blue**, our responses are in **black**, and modifications of the original manuscript are highlighted in **yellow** in the revised manuscript.

This manuscript by Sheng et al. describes a 3-year ammonia product retrieved over Asia from geostationary thermal IR spectrometer GIIRS aboard the FengYun-4 satellite. The retrieval is based on the FY-GeoAIR algorithm developed by the same group in a 2023 AMT paper (Zeng et al., 2023, https://doi.org/10.5194/amt-16-3693-2023). This work comprehensively compares GIIRS ammonia column amount with temporally matched counterparts from IASI and CrIS. The GIIRS columns are also evaluated against ground-based FTIR measurements in Hefei in east China. Seasonal and diurnal patterns are presented with the focus on a few source regions in north/southwest China and south Asia. The spatiotemporal patterns observed by GIIRS are compared with the MIX emission inventory and GEOS-CF CTM simulation, with significant differences noted. This paper presents quite solid work, and the ammonia retrieval from a geostationary hyperspectral imager is a significant advancement from the prior work. The authors may consider the following comments for further improvements of this manuscript.

Response: We thank the reviewer for thorough review and constructive suggestions. As you are concerned, there were several issues that need to be addressed. We have made major and careful modifications to the original manuscript according to all the comments and suggestions from the reviewers. The main modifications are summarized as follows:

(1) GIIRS NH_3 retrieval algorithm and data comparison. A detailed description of the retrieval algorithm has been added in the appendix, including the the interpretation and calculation of column averaging kernel (AVK). We also clarified the data coverage in Fig. 1 and added Fig. S2 to illustrate the impact of the thermal contrast (TC) filtering on data availability.

(2) Text revisions and additional references. Some paragraphs and sentences have been rewritten for improved clarity and completeness. Additional references have been included to strengthen the discussion, including those related to geostationary satellite observations, the reliability of the MIX emission inventory, and NH_3 emission studies over the Sichuan Basin.

(3) Figure revisions and optimization. Several figures have been refined and simplified to reduce redundancy, particularly Fig. 1 and Figs. 12–14. The definition of the study regions has been made clearer. Figure 1 now highlights the three key regions discussed in the manuscript, while Fig. S4 shows locally enhanced areas. Figure S16 presents the selection of eight major agricultural areas, and Figs. 11–14 display the spatial and temporal distributions of daytime NH_3 variations.

Please see our responses, and associated changes in the revised manuscript, to your comments and suggestions below.

The main general comment is about how the retrieval of this product differs from the algorithm paper, Zeng et al. (2023) and related, the consistency of using averaging kernel to quantify vertical sensitivity of the retrieved column. The algorithm paper fully resolves ammonia and water vapor profiles as 11 separate layers, whereas the current manuscript, presumably will serve as a data product paper, scales a single a priori ammonia profile. This implies that there is only one state vector element for ammonia, instead of 11. This appears to be a significant change of the retrieval setting, which should be better justified, evaluated, and augmented by details of the current retrieval setting and how these differ from the algorithm paper. The details of this retrieval are arguably more important than those in the algorithm paper for the users of this product.

Response: Thank you for your insightful comment and constructive suggestion. We have added the descriptions for the change of the retrieval setting in this study in comparison to Zeng et al. (2023a):

"In this study, the retrieval configuration and parameters are identical to those described in Zeng et al. (2023a), except that a profile-scaling retrieval approach was adopted instead of the full-profile retrieval method. The full-profile retrieval method fully resolves the ammonia profile as 11 separate layers. In contrast, the profile-scaling retrieval approach only retrieves the total column of NH_3. It applies a single representative a priori profile (identical for all scenes) and scales this profile in the retrieval algorithm to optimize the spectra fitting. In this case, there is only one state vector element for NH_3, instead of 11. The reasons for this change of the retrieval configuration are: (1) the degrees of freedom for signal (DOFS) for most NH_3 retrievals as shown in Zeng et al. (2023a) is less than one, indicating less than one piece of information is available from the spectra for NH_3 and not sufficient to constrain its vertical distribution; (2) using the profile-scaling retrieval approach speeds up the retrieval calculation. Similarly, only total column is retrieved for the interference gas H_2O. The retrieval yields the NH_3 column and

the posteriori error estimate. In addition, the column averaging kernel (AVK) is derived simultaneously in the optimal estimation framework. The column AVK value at a given atmospheric layer represents the change in the retrieved total NH_3 column with respect to a perturbation of the partial NH_3 column at that layer. It therefore reflects the height-dependent sensitivity determined by the temperature difference between the surface and the given atmospheric layer (Fig. A1 and Fig. S1). This definition of AVK is similar to that from the Total Carbon Column Observing Network (Wunch et al., 2011) and IASI (Clarisse et al., 2023), but differs from conventional matrix AVK from optimal estimation (Shephard et al., 2011, 2015). Further details on interpretation and calculation of the column AVK are provided in the Appendix."

Please see our responses to your next comment on the calculation of column averaging kernel.

A related issue is the averaging kernel and the vertical sensitivity of the product. In general, this manuscript may benefit from more discussion and presentation on this topic, as the diurnal coverage and diverse spatial coverage likely lead to large variations of vertical sensitivity. Namely, the lack of interesting signals in some time/place may be due to weak sensitivity to near-surface concentration. By switching from profile to single scaling factor retrieval, this manuscript seems to (partially) move from the optimal estimation view of averaging kernel, as in Zeng et al. 2023 and CrIS algorithm papers, to the DOAS view of averaging kernel as in the IASI v4 paper (Clarisse et al., 2023, https://doi.org/10.5194/amt-16-5009-2023). This could lead to profound confusion without detailed clarification. The "column averaging kernel" discussed in Section 2.1.1 and Fig. S1 seem to be the DOAS AVK, not the optimal estimation AVK. The actual "column averaging kernel", in optimal estimation, is also a vector calculated from the averaging kernel matrix (e.g., see Eq. 8 in Connor et al., 2008, https://doi.org/10.1029/2006JD008336). The text definition in lines 151-153 of this manuscript seems to match the optimal estimation column averaging kernel, not the DOAS one shown in Fig. S1a. Figure S1 actually shows both DOAS (panel a) and optimal estimation AVKs (panel c) without clear distinction. The authors, which include developers of both IASI and CrIS algorithms, are encouraged to disentangle this issue.

Response: Thank you for this insightful and technically important comment. We agree that averaging kernels and vertical sensitivity are critical for interpreting the retrieval results. We have added the following descriptions in the Appendix to define the column AVK from this study, described the calculation of AVK, and compared the results using numerical calculation.

Appendix: The interpretation and calculation of column AVK

In the profile-scaling optimal estimation framework, the column AVK (unitless) represents the change in the retrieved total NH_3 column (molec/cm^2) with respect to a perturbation of the partial NH_3 column (molec/cm^2) at a given atmospheric layer. For example, if the true NH_3 partial column in the first layer near the surface increases by 1.0×10^{16} molec/cm^2, whereas the retrieval algorithm only detects an increase of 0.4×10^{16} molec/cm^2 in the final retrieved total column, the resulting column AVK for the first layer is 0.4. A value of 1.0 would imply perfect sensitivity to that layer. As a hyperspectral sounder has varying sensitivities to different altitudes and the spectral signatures of NH_3 molecules vary at different altitudes, the retrieved total column is not uniformly sensitive to NH_3 molecules at all heights. The one-dimensional column AVK thus provides a crucial diagnostic metric to understand where the retrieved column information is originating. This definition of column AVK is conceptually similar to that from TCCON (Wunch et al., 2011) and IASI (Clarisse et al., 2023). By contrast, the conventional matrix AVK from optimal estimation quantifies how much information is retrieved from the measurement (Shephard et al., 2011, 2015), and the sum of each row of AVK provides an estimate of the fraction of retrieval information contributed by the measurement rather than the a priori at the corresponding altitude. When the information content of the measurement is high or the retrieval loosely constrained, the AVK values approach the unit matrix. Conversely, when the information content is low or the retrieval is heavily constrained, the AVK values tend toward zero and the solution remain close to the a priori. A detailed discussion on the difference between column AVK and matrix AVK can be referred to Clarisse et al. (2023).

The column AVK is calculated following the formalism of the full matrix AVK from optimal estimation, which is expressed as:

$$\text{Column AVK} = \mathbf{G}\,\mathbf{K}_{GasProf} \tag{A1}$$

where $\mathbf{K}_{GasProf}$ is the layer-resolved NH_3 Jacobian quantifying the sensitivity of radiance to layer-specific NH_3 partial column perturbations. $\mathbf{K}_{GasProf}$ is calculated using the radiative transfer model for each retrieval. The gain matrix G is given by:

$$\mathbf{G} = (\mathbf{K}_{col}{}^{T}\mathbf{S}_{\varepsilon}{}^{-1}\mathbf{K}_{col} + \mathbf{S}_{a}{}^{-1})^{-1}\mathbf{K}_{col}{}^{T}\mathbf{S}_{\varepsilon}{}^{-1} \tag{A2}$$

where $\mathbf{K}_{col}$ is the total-column NH_3 Jacobian quantifying the sensitivity of radiance to total NH_3 column, $\mathbf{S}_{\varepsilon}$ and $\mathbf{S}_{a}$ are the noise covariance matrix for the measured radiances and the a priori covariance matrix for the retrieval.

To verify the analytical column AVK calculated from Eq. (A1), observation simulation experiments were conducted to calculate the corresponding numerical

column AVK for comparison. An observation over the North China Plain (41.97°N, 122.50°E) on 15 July 2025 was selected, with a surface pressure of 1002.65 hPa, surface temperature of 302.49 K, and lowest-layer air temperature of 297.46 K. The "true" NH_3 profile was generated by scaling the a priori profile from Zeng et al. (2023a) by a factor of 10 (approximate total column: 9.49×10^{16} molec/cm^2), which was also used as the a priori profile for all retrievals. We first simulated the "true" radiance spectrum from the "true" profile, added Gaussian random noise, and ran the retrieval algorithm 100 times to obtain the mean retrieved total column, which is close to the true total column. The analytical column AVK solution from this observation was then derived using Eqs. (A1) and (A2). Subsequently, we performed a layer-wise perturbation test to derive the numerical column AVK. A fixed NH_3 perturbation of 1×10^{16} molec/cm^2 was individually added to each of the 12 retrieval layers of the "true" profile, while keeping all other layers unchanged. For each perturbed layer, the noise-added retrieval was repeated 100 times to obtain the mean retrieved total column. The numerical column AVK was then calculated as the ratio of the retrieved total column change to the imposed "true" column increment (1×10^{16} molec/cm^2). Figure A1 compares the analytical and numerical AVKs, showing good agreement between the two sets, thereby justifying the calculation of column AVK using Eqs. (A1) and (A2).

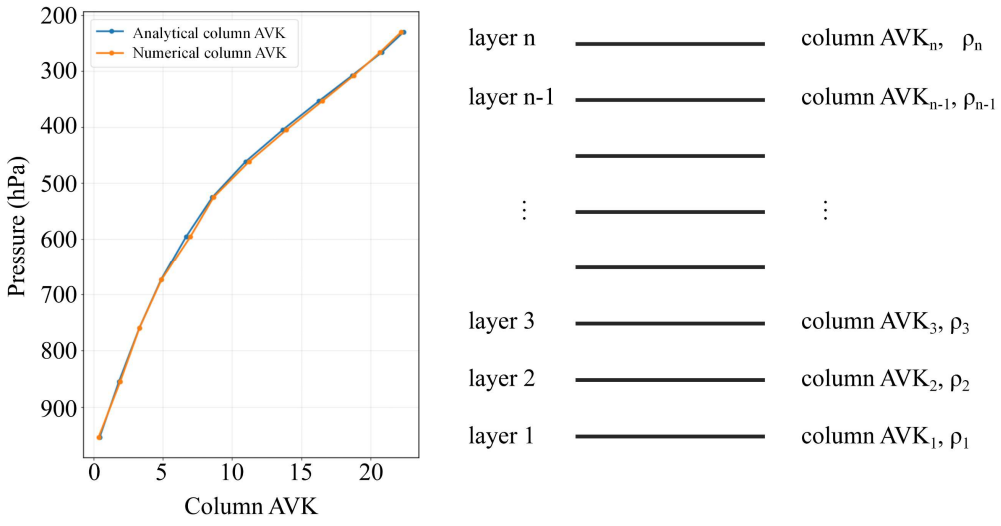

Figure A1. Left panel: Example of the analytical and numerical column AVK over the North China Plain on 15 July 2024. Right panel: Schematic of the retrieval vertical layers (from surface to 200 hPa). The number of retrieved pressure levels is denoted by n (n=11 or 12 in most cases). The column AVK value (column AVK $_i$) and the air density (ρ) of NH_3 at each layer are also indicated.

Secondarily, the authors may think about the consistency of GIIRS, IASI, and CrIS filtering for the intercomparisons. Each comparison point, e.g., in Figs. 3 and 4, are averaged from a number of soundings for each instrument. Uncoordinated

filtering schemes according to each instrument's recommendation may lead to relative biases in sampling and sampling-induced differences even when they actually measure the same value at the same sounding location/time. For example, the GIIRS data filters negative values (line 158), but IASI allows negative (line 183). Ideally, the strictness of filtering should be comparable, or even better, the soundings are matched at individual overpass level.

Response: Thank you for your thoughtful and constructive comment. Because the GIIRS, IASI, and CrIS retrievals are based on different algorithms and error characterizations, we applied the recommended quality filtering criteria for each dataset to ensure the reliability of the individual products. CrIS retrieval is performed in logarithmic space to span the large dynamic range of NH_3, which inherently avoids negative values. IASI uses an HRI-based machine learning retrieval method, and negative values are suggested to be retained to ensure un-biasness when doing averaging. NH_3 retrieval is based on the Artificial Neural Network for IASI (ANNI) framework, in which negative values may arise from observational noise or near-zero background conditions. After applying the recommended quality filtering criteria, non-physical negative values caused by errors in input parameters and anomalous radiative transfer are removed, while statistically consistent negative values within the expected noise distribution are retained. This treatment avoids introducing a positive bias under low-concentration conditions, helps ensure the accuracy of the retrieval results, and preserves a realistic representation of background conditions. In addition, the CrIS and IASI datasets have been extensively validated in previous studies. For GIIRS retrieval, negative values may occur because the inversion is performed in linear space, and noise can drive retrieved values below zero when the true NH_3 concentration is close to the detection limit. These values are non-physical and are therefore removed.

The comparisons shown in Figs. 3–4 are intended as an initial evaluation of the overall consistency among the satellite datasets. As further discussed in the manuscript, we additionally consider the impact of vertical sensitivity using averaging kernels and perform consistency analyses over selected regions (e.g., the North China Plain and the Northeast China Plain), where the influence of sampling differences is reduced.

To further improve the robustness of the intercomparison, we have revised the analysis for Figs. 3–4 by applying consistent collocation criteria across the three instruments. Specifically, satellite observations are now matched using the same overpass time and location constraints, with temporal differences within 1 hour and spatial differences within 0.5° grid cells. The updated results are very similar to the original figures, indicating that the conclusions are robust and not sensitive to the collocation and filtering differences.

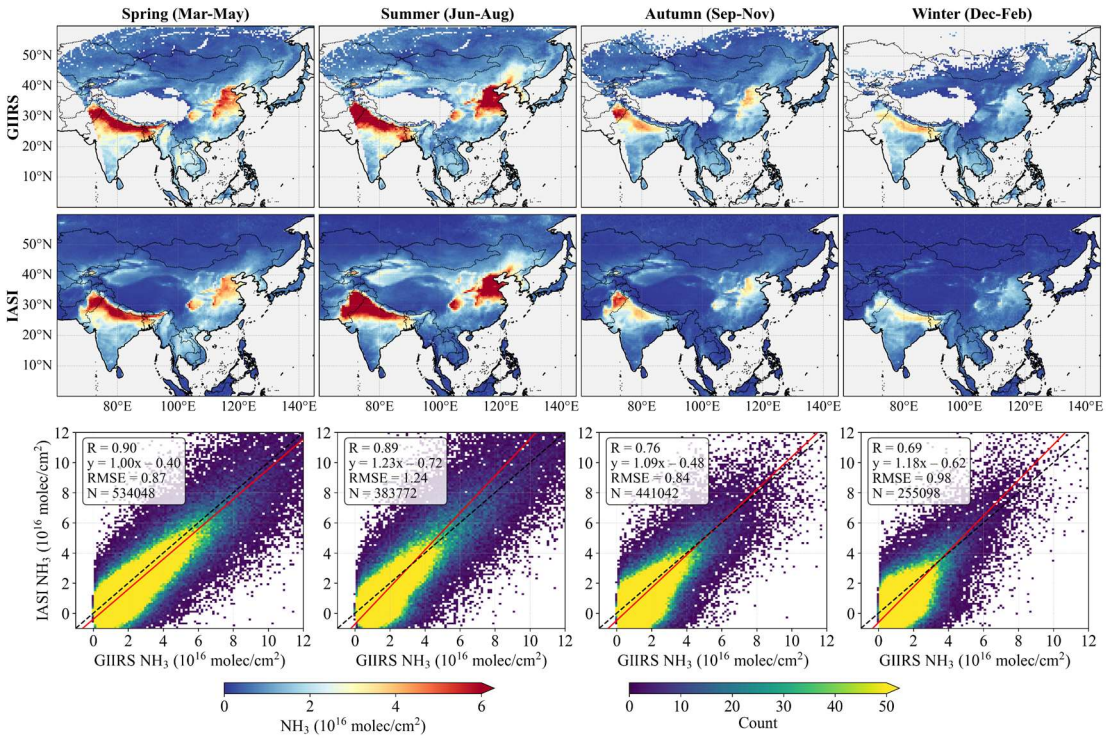

Figure 1. Comparison of NH_3 columns observed by GIIRS and IASI during morning overpasses (~09:30 LST) from July 2022 to June 2025. Seasonal maps are presented on a 0.5° × 0.5° grid. Scatter plots compare GIIRS and IASI data matched by overpass times within 1 hour and spatial locations within the same 0.5° × 0.5° grid cells.

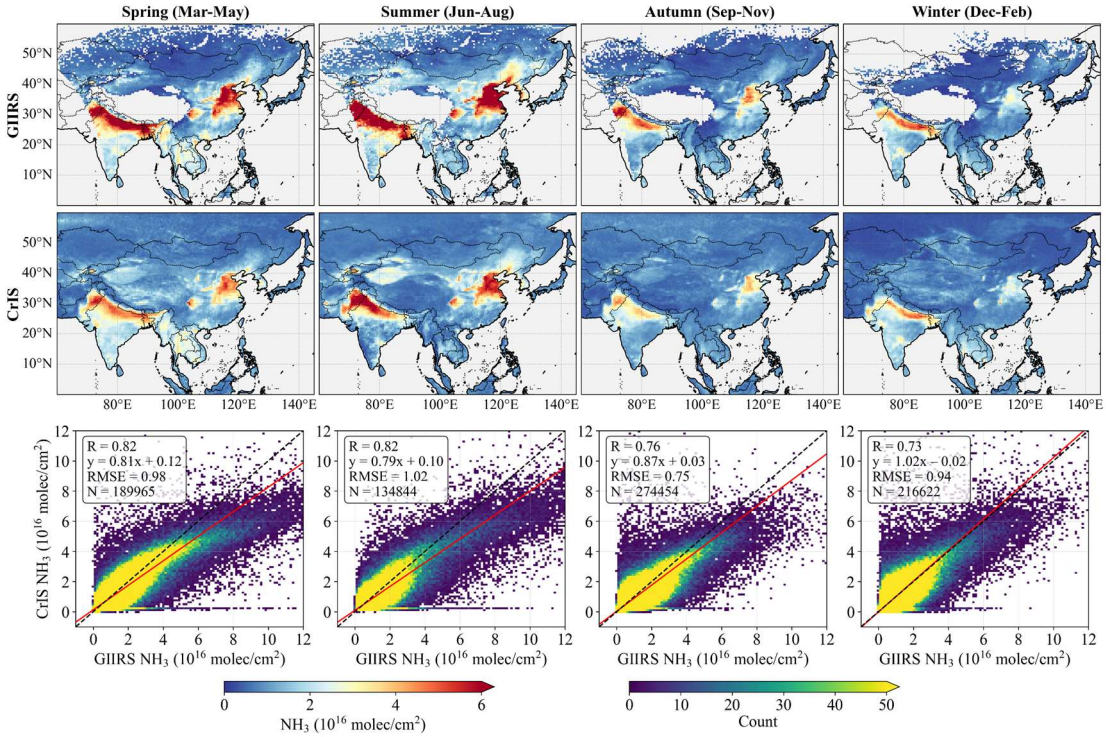

Figure 2. Comparison of NH_3 columns observed by GIIRS and CrIS during afternoon overpasses (~13:30 LST) from July 2022 to April 2025. Seasonal maps are presented on a 0.5° × 0.5° grid. Scatter plots compare GIIRS and CrIS data matched by overpass times within 1 hour and spatial locations within the same 0.5° × 0.5° grid cells.

Last, the authors may consider enhancing the comparison with a CTM (GEOS-CF is already presented over a short time period). It seems convincing that GIIRS/IASI/CrIS/FTIR agree reasonably well, with caveats noted in the previous two main comments. However, limited data-model comparisons (Fig. 6 and Fig. 15) indicate that the CTM world is very far away from observations. To the degrees feasible, the authors are encouraged to trade some of the similar maps that take large space (Figs. 2-4, 7, 12-14, S3, S16-18, S20-22) with maps that highlight the spatial/temporal differences between measured and simulated columns.

Response: Thanks for this valuable suggestion. Comparisons with chemical transport models (CTMs), such as GEOS-CF, are important for evaluating the consistency between satellite retrievals, as discussed in Sect. 3.1. The data-model comparisons in Fig. 15 and Fig. S21–24 indicate that the GEOS-CF tends to underestimate or otherwise differ from observations in certain regions and periods. In addition, comparisons of Fig. 11–14 and Fig. S25–28 specifically highlight the spatial and temporal differences between the observed satellite columns and the GEOS-CF simulated columns. These figures allow a more direct assessment of model performance relative to the observations, without removing the key information previously presented.

In the revised manuscript, we have simplified several figures to reduce redundancy, particularly Fig. 1 and Figs. 12–14, while retaining other figures that contain important information for understanding the spatial and temporal patterns of NH_3.

Minor comments:

Line 38: it is unclear how the timing shifts from north to south.

Response: Thanks for pointing this out. In the revised manuscript, we have rephrased the statement.

"The NH_3 peaks occur between March and July, with peak timing earlier in the south and later in the north, reflecting regional differences primarily driven by agriculture activities."

Lines 55-56: unclear how ammonia can influence source and sink of methane in any significant way. It does not appear in the reference.

Response: Thanks for your thorough review. We agree that the previous statement regarding the influence of NH_3 on methane sources and sinks was not sufficiently supported by the cited reference and could be misleading.

The sentence was intended to describe the indirect climatic effects of NH_3 through aerosol-mediated changes in atmospheric oxidative capacity. However, this mechanism

is not explicitly addressed in the cited reference. To avoid overinterpretation, we have removed the discussion of methane and revised the sentence as follows:

"NH_3 also exerts indirect influences on global climate change, for example, by driving nitrous oxide (N_2O) formation via atmospheric oxidation (Pai et al., 2021) and by altering radiative forcing through aerosol-mediated processes (Gong et al., 2024)."

Gong, C., Tian, H., Liao, H., Pan, N., Pan, S., Ito, A., Jain, A. K., Kou-Giesbrecht, S., Joos, F., Sun, Q., Shi, H., Vuichard, N., Zhu, Q., Peng, C., Maggi, F., Tang, F. H. M., and Zaehle, S.: Global net climate effects of anthropogenic reactive nitrogen, Atmos. Chem. Phys., 24, 557–563, https://doi.org/10.1038/s41586-024-07714-4, 2024.

Pai, S. J., Heald, C. L., and Murphy, J. G.: Exploring the global importance of atmospheric ammonia oxidation, ACS Earth Space Chem., 5, 1674–1685, https://doi.org/10.1021/acsearthspacechem.1c00021, 2021.

Line 63: probably inaccurate to name Asia as a hot "spot".

Response: Thanks for pointing this out. We have rephrased the statement as follows:

"Asia is the world's most significant NH_3 emission regions, accounting for over 30% of global NH_3 emissions annually as reported by the Emissions Database for Global Atmospheric Research (EDGAR) inventory."

Line 93: EDGAR should be defined at first appearance.

Response: Thanks for your pointing this out. We have added the definition in the revised manuscript.

Line 108: check if the ammonia, not the CO algorithm paper, should be cited here.

Response: Thanks for noticing that. In the revised manuscript, we have corrected the citation to refer to the ammonia retrieval algorithm paper (Zeng et al., 2023a).

Zeng, Z.-C., Lee, L., Qi, C., Clarisse, L., and Van Damme, M.: Optimal estimation retrieval of tropospheric ammonia from the Geostationary Interferometric Infrared Sounder on board FengYun-4B, Atmos. Meas. Tech., 16, 3693–3713, https://doi.org/10.5194/amt-16-3693-2023, 2023a.

Line 117: MIX should be defined.

Response: Thanks for your suggestion. We have added the definition in the revised manuscript. The revised sentence now reads:

"The spatial patterns and seasonal cycles of NH_3 observed by GIIRS are compared with observations from IASI and CrIS, as well as estimates from the mosaic Asian anthropogenic emission inventory (MIX) in Sect. 3.1."

Figure 1: the ABCD boxes seem to be arbitrary and do not correspond to particular agricultural regions. Suggest some text on how they are selected.

Response: Thanks for your question and suggestion. The boxes are located in three major agricultural regions characterized by high NH_3 concentrations, high anthropogenic emissions, and flat cropland.

In the original manuscript, Sect. 3.3 (first paragraph) describes these areas as follows: "We focused on eight major agricultural source areas with a high proportion of irrigated cropland, located in the North China Plain and the Northeast China Plain, the Sichuan Basin, and the Indo-Gangetic Plain (black boxes in Fig. 1), to further investigate daytime variations in NH_3 columns."

In the revised manuscript, we have rephrased this description for clarity and labeled these emission areas in Fig. S16 to make them more easily identifiable to readers.

The revised sentence now reads: **"We focused on eight major agricultural source areas with a high proportion of irrigated cropland, located in the North China Plain and the Northeast China Plain, the Sichuan Basin, and the Indo-Gangetic Plain (black boxes in Fig. 1), to further investigate daytime variations in NH_3 columns."**

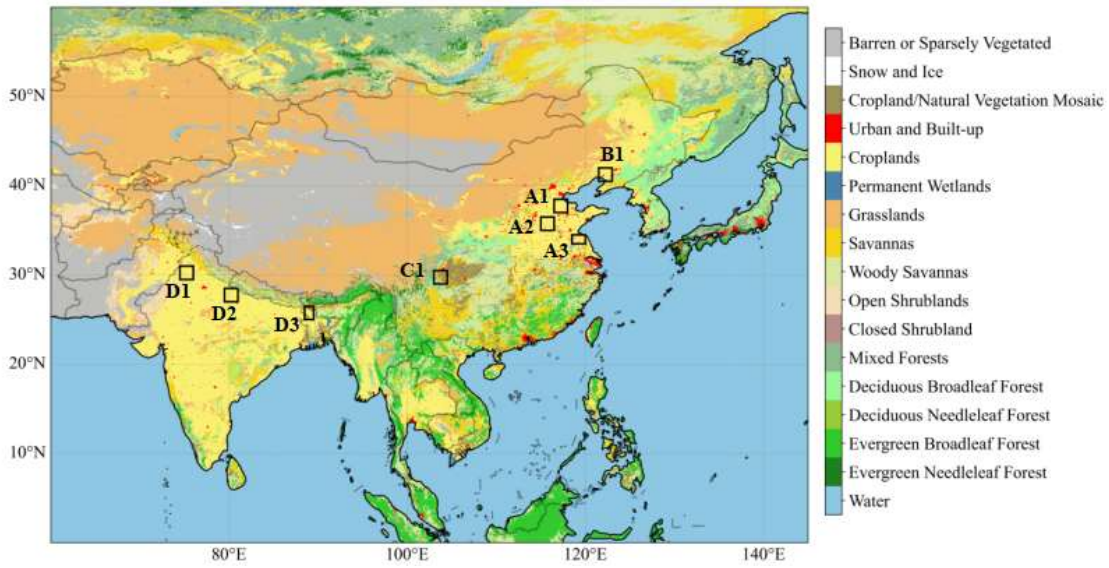

Figure S1. Spatial distribution of land cover over East Asia in 2025 based on the Moderate Resolution Imaging Spectroradiometer (MODIS) MCD12C1 dataset (https://ladsweb.modaps.eosdis.nasa.gov/, accessed March 19 2026). Black boxes indicate the eight agricultural source areas analyzed in Sect. 3.3.

Figure 1: showing a bottom up inventory might be a missed opportunity to present an all-time, high resolution map of the entire GIIRS data set. Consider labeling the source regions that appear in the main text (lines 261-263, 508-509) but only in

supplement figure (Fig. S3).

Response: Thanks for your suggestion. To keep Fig. 1 concise, we have only outlined three major source regions: the North-Northeast China Plains, the Sichuan Basin, and the Indo-Gangetic Plain. These regions are the main areas of interest in this study. The other source regions mentioned in the main text are indicated in Supplementary Fig. S4.

In the revised manuscript, the text is as follows: **"Elevated NH_3 columns, significantly above background levels, are observed over the Indo-Gangetic Plain, the North China Plain, the Sichuan Basin, and the Northeast China Plain (as shown by the black boxes in Fig. 1). The daytime NH_3 columns reach values exceeding 4×10^{16} molec/cm^2, primarily driven by intensive agricultural activities and supplemented by non-negligible contributions from urban and industrial emissions. Localized weaker enhancements of NH_3 column concentrations are evident over agricultural core areas in China (including the Ningxia Irrigation Plain, the Wei River Plain, the Jianghan Plain, and oasis agriculture in the arid regions of Xinjiang), as well as the central Deccan Plateau in India, the Mekong Delta in Vietnam, the Chao Phraya River Plain in Thailand, and the Fergana Valley in Uzbekistan (as shown by the dashed boxes in Fig. S4)."**

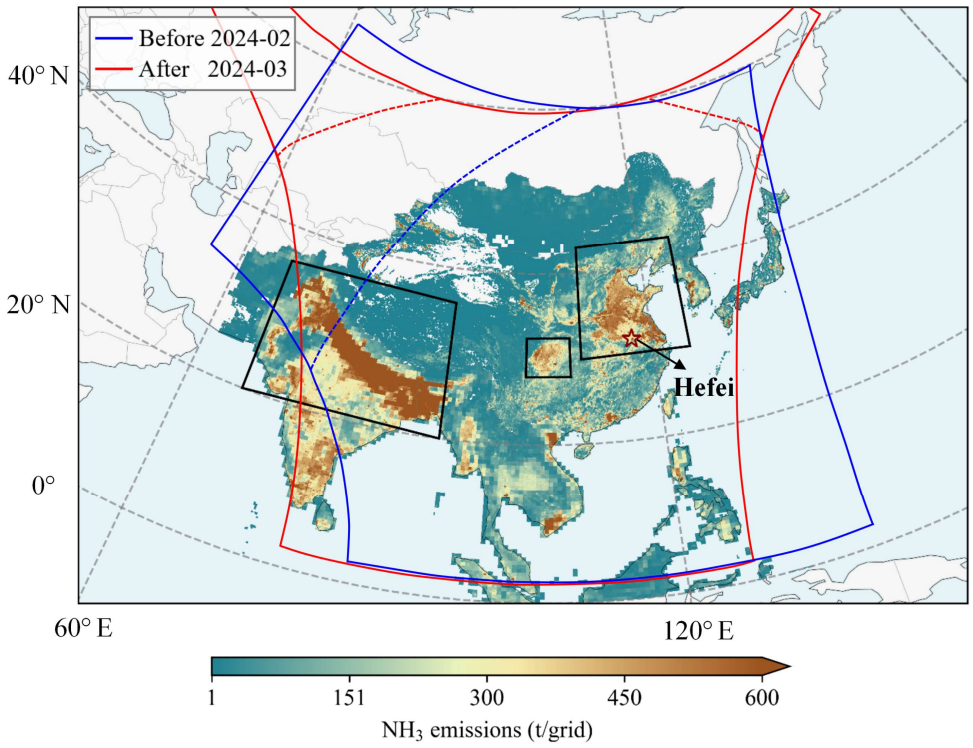

Figure 3. Spatial domain of FY-4B/GIIRS observations and NH_3 retrievals over East Asia. Blue and red solid lines outline GIIRS observational coverage before and after the FY-4B orbital relocation, respectively. Blue and red dashed lines denote the corresponding NH_3 retrieval domains, with viewing zenith angles greater than 70° excluded. The background map shows total anthropogenic NH_3 emissions in 2017 from the MIXv2 emission inventory at a 0.1° grid resolution (Li et al., 2024). The red pentagram marks the location of the

Hefei station, which is further described in Sect. 3.2. Black boxes outline major agricultural areas, including the North-Northeast China Plains, the Sichuan Basin, and the Indo-Gangetic Plain.

Lines 155-158: do these criteria effectively remove non-detects like the CrIS product (lines 197-199)? Is it fair to say that GIIRS and CrIS exclude non-detects but IASI include them? How does that influence the instrument comparison?

Response: Thank you for your insightful question. In fact, the new version of the CrIS dataset adopts a very detailed approach to account for non-detects in order to avoid introducing a high bias in the results. Therefore, the filtering criteria used in this study do not remove non-detects. To clarify this point, we have added the following statement in the revised manuscript: **"The dataset utilizes the information content of the satellite measurements to explicitly identify and account for cloud-free observations below the sensor detection level (White et al., 2023)."**

Because the three satellite data products are based on different retrieval algorithms and error characterizations, we applied the quality filtering criteria recommended for each dataset, as described above. Our analysis mainly focuses on regions with strong anthropogenic emissions, where pronounced positive NH_3 columns are observed. In these high-concentration areas, the signal-to-noise ratio is high, and the influence of non-detects or negative values is minimal. In addition, we conducted sensitivity tests using different filtering strategies (e.g., excluding negative IASI values or applying more relaxed thresholds for GIIRS), and the resulting spatial patterns and inter-sensor comparisons changed only marginally. This indicates that, based on the recommended filtering criteria already applied, differences in quality filtering among GIIRS, CrIS, and IASI have a limited impact on the conclusions of this study.

Line 210: fix "showing broadly consistent with"

Response: Thank you for pointing this out. We have rephrased the sentence for grammatical clarity as follows: **"Previous study has demonstrated that FTIR measurements at Hefei effectively capture the spatiotemporal variability of NH_3 columns, and the retrievals are broadly consistent with IASI satellite data (Wang et al., 2022)."**

Figure 3: the axis limits should show negative values. Since the retrieval operates in linear space, instead of log space like CrIS, negative values are meaningful results. It is questionable to remove them, which will bias the mean value high.

Response: Thanks for your comment. In the GIIRS NH_3 retrievals, negative values primarily reflect retrieval noise rather than physically meaningful concentrations. These negative values are filtered out in our analysis. In the revised manuscript, we further

improved the consistency of the intercomparison by applying strict co-location criteria, using the same overpass time and spatial matching conditions for all datasets to minimize potential biases associated with sampling mismatch and differences in data filtering (e.g., treatment of negative values).

Moreover, our study focuses on regions with high NH_3 columns driven by anthropogenic emissions. Therefore, the exclusion of negative values has minimal impact on the results and comparisons presented.

Figure 6: presumably these are ammonia column enhancements calculated by subtracting the regional background fitted by Eq. 1, i.e., these are enhancements, not just GIIRS columns. The comparison between column (mol/m2) with emission is largely qualitative than quantitative, because the seasonality of column could be quite different from column-derived emissions (see Figs. 10-11 in Li et al. 2026, https://doi.org/10.5194/acp-26-703-2026). Does the enhancement calculation go one step further from column to emission? If so, it could be used to justify section 2.5 and Fig. 6.

Response: Thanks for your help comment. Figure 6 presents regional NH_3 column concentrations, which are derived using the curve-fitting method described in Sect. 2.5.1, rather than column enhancements. This figure is used to illustrate the seasonal variations of NH_3 columns and anthropogenic emissions for each region.

In the revised manuscript, we added Fig. S8 in the Supplement to compare the seasonal cycles of NH_3 columns and emissions, highlighting the temporal mismatch between them. We have clarified in the manuscript that the comparison in Fig. 6 is qualitative and does not imply a direct conversion from column variations to emissions.

The related description is as follows: **"Several studies have reported that NH_3 emissions inferred from satellite observations exhibit distinct seasonal variations that can differ from those of the NH_3 columns (Kumar et al., 2025; Li et al., 2026). Therefore, we focus on the spatial distribution of NH_3 enhancements, relative to regional background levels, as captured by different satellites."**

Kumar, P., Broquet, G., Hauglustaine, D., Beaudor, M., Clarisse, L., Van Damme, M., Coheur, P., Cozic, A., Zheng, B., Revilla Romero, B., Delavois, A., and Ciais, P.: Global atmospheric inversion of the anthropogenic NH3 emissions over 2019–2022 using the LMDZ-INCA chemistry transport model and the IASI NH3 observations, Atmos. Chem. Phys., 25, 12379–12407, https://doi.org/10.5194/acp-25-12379-2025, 2025.

Li, Z., Sun, K., Guan, K., Wang, S., Peng, B., Clarisse, L., Van Damme, M., Coheur, P.-F., Cady-Pereira, K., Shephard, M. W., Zondlo, M., and Moore, D.: Ammonia emissions and depositions over the contiguous United States derived from IASI and CrIS using the directional derivative

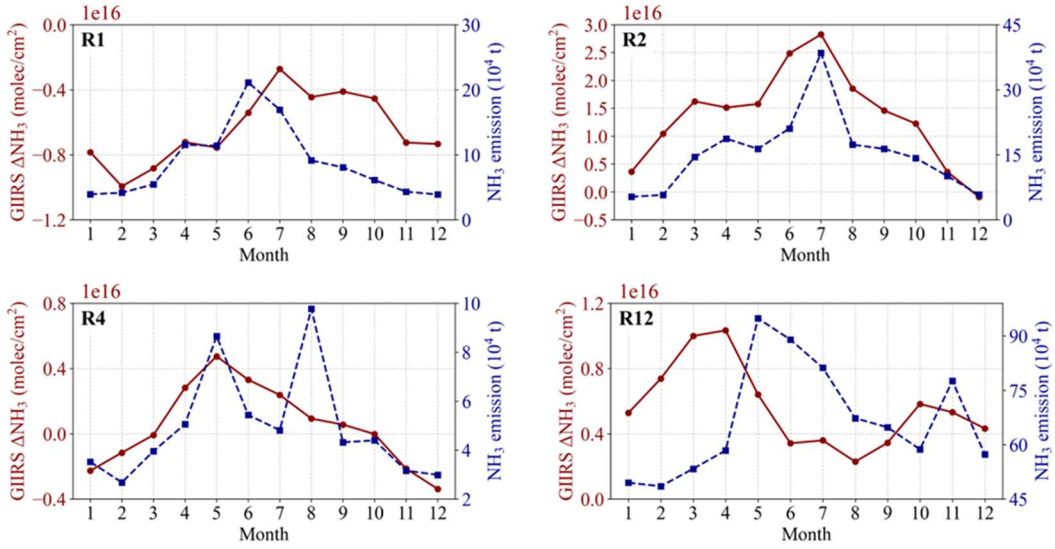

Figure S2. Comparison of seasonal cycles of GIIRS-observed NH_3 columns and MIX-based NH_3 emissions. ΔNH_3 are regional NH_3 variations relative to the background level over East Asia, primarily reflecting concentration changes associated with local anthropogenic emissions and meteorological conditions. The four regions correspond to the subregions defined in Fig. 6.

Line 327: please elaborate what "data discrepancies" are.

Response: Thanks for your comment. The term "data discrepancies" refers to the differences among satellites arising from variations in local overpass times and sensor sensitivities of polar-orbiting and geostationary satellites. To improve clarity, we have reorganized the paragraph and explicitly specified the sources of these inter-satellite differences. The revised text now reads as follows: **"Due to data discrepancies in local overpass times and sensor sensitivities among the polar-orbiting and geostationary satellites (Shephard et al., 2025), the enhancement values detected by CrIS are 0.50 ± 0.64 and 0.74 ± 0.90 $\times 10^{16}$ molec/cm^2 lower than those detected by GIIRS and IASI, respectively. These inter-satellite differences can lead to inconsistencies in the observed NH_3 enhancements across various source regions, particularly in the Sichuan Basin, the Ningxia Irrigation Plain, and the urban and biomass-burning regions of Southeast Asia."**

Figure 7: I wonder if it is more effective to present the difference maps (e.g., IASI subtracting GIIRS). A general comment about figures is that there are so many maps that are very similar and hard to identify informative spatial pattern.

Response: Thank you for your thoughtful suggestion. In Fig. 7, our primary objective is to compare the spatial distribution of NH_3 enhancements detected by different satellite datasets after applying a consistent background removal approach. Because the

absolute NH_3 column concentrations and the corresponding background values differ between GIIRS and IASI, directly comparing the differences in column concentrations (e.g., IASI minus GIIRS) may not provide a meaningful interpretation. Instead, using the same background-removal method allows us to focus on the relative enhancement regions identified by each instrument. After careful consideration, we therefore decided to retain the current presentation of Fig. 7, as it better serves the purpose of highlighting the spatial distribution of satellite-detected NH_3 enhancements.

Lines 348 and 352: the Pearson correlation coefficient only depends on x and y data, not on a regression model. Should a coefficient of determination (R2) used here?

Response: Thanks for your suggestion. In the revised manuscript, we have updated the statistics in Sect. 3.2 for the cross-comparison figures by replacing the Pearson correlation coefficient with the coefficient of determination (R^2). In addition, we have added the uncertainties of the regression slopes to provide a more complete statistical characterization.

Line 360: unclear how can GRIIS be "most" reliable across all daytime hours?

Response: Thanks for your question. The original sentence was somewhat misleading. In fact, the reliability of GIIRS NH_3 retrievals varies within the daytime period. Specifically, retrievals are generally more reliable during daytime hours (07:00–19:00 LST) than at night, and are most reliable when the thermal contrast (TC) exceeds 5 K. To clarify this point, we revised the text in the manuscript.

In Sect. 2.1.1 (Data description), we added an explanation for the use of daytime observations. The revised text reads:

"In this study, NH_3 retrievals from individual observations over land during daytime (7:00–19:00 LST) were utilized to investigate spatial and temporal variations over East Asia (Fig. 2), whereas nighttime data were excluded due to insufficient thermal contrast."

In Sect. 3.2, the original sentence has been revised to: **"GIIRS NH_3 column retrievals are most reliable when TC exceeds 5 K, a condition predominantly observed during summer daytime hours (07:00–19:00 LST). "**

Line 436: clarify what "fixed locations" means.

Response: Thanks for your suggestion. Here, "fixed locations" refers to the relatively stable spatial distribution of major agricultural emission sources, such as croplands and large-scale livestock facilities, in the Northeast China Plain. Because these sources are

geographically stable and emissions are spatially concentrated, the spatial pattern of NH_3 concentrations shows little variation at different local times. To clarify this point, the sentence has been revised in the manuscript.

"Because agricultural emission sources are spatially concentrated and geographically stable, the spatial pattern of NH_3 enhancements shows little variation at different local times (Fig. 12)."

Line 492: should be Figs. S19-22.

Response: Thanks for pointing this out. The relevant figures and their references have been updated in the revised manuscript. We also carefully checked and updated the figure numbering throughout the manuscript to ensure consistency.

Figure S1: the caption is very confusing and should be revisited. It does not seem to match each panel, with AVK notations mixed as pointed in the first main comment.

Response: Thanks for pointing this out. In the revised manuscript, the caption of **Fig. S1** has been carefully rewritten to ensure that the descriptions clearly correspond to each panel. In addition, an explicit explanation of the AVK notation has been added to improve clarity and avoid potential confusion (**Text S1**).

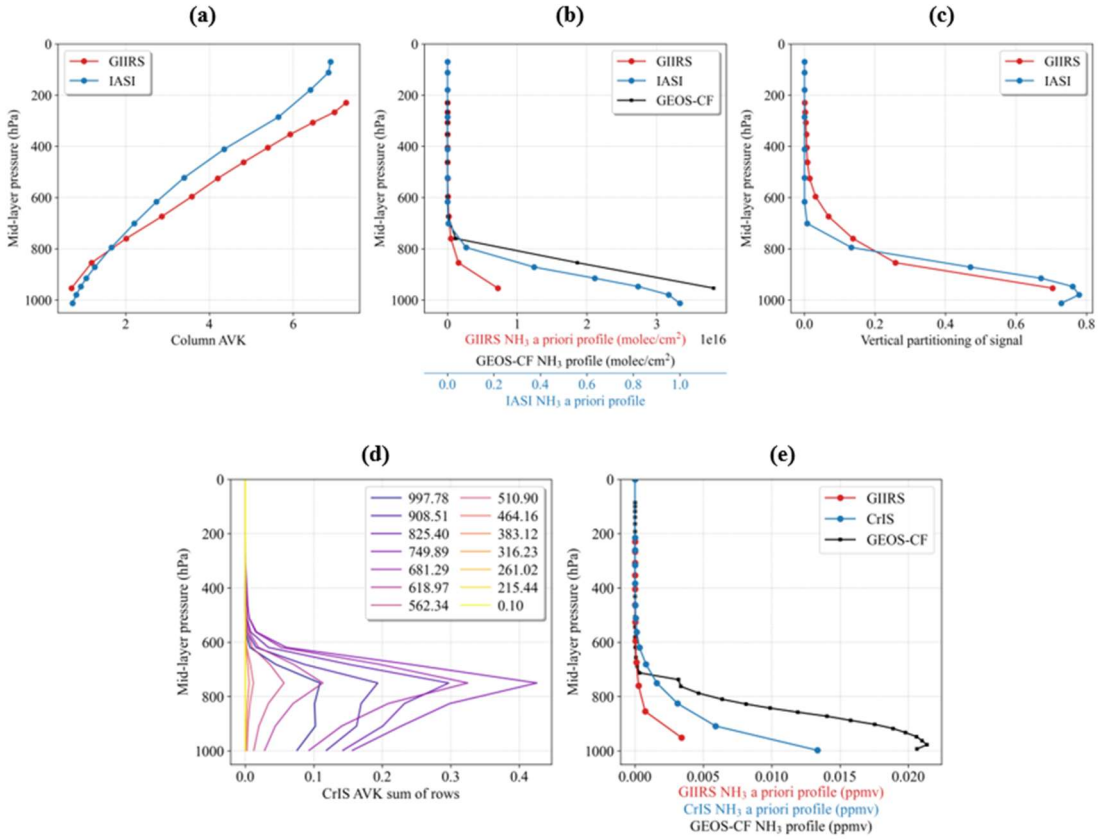

Figure S3. Illustration of satellite's AVKs and a priori profiles using two example retrievals over the North China Plain. Top panels show GIIRS and IASI observations near 38.35°N, 116.82°E on 9 June 2024. (a) Column AVKs from GIIRS and IASI. (b) The corresponding a priori profile from GIIRS and IASI, compared with GEOS-CF NH_3 profile, which have been interpolated onto GIIRS' retrieved layers. (c) Vertical partitioning signals of GIIRS and IASI, obtained by multiplying the column AVK with the normalized a priori profile. Bottom panels show GIIRS and CrIS observations near 38.04°N, 117.67°E on 14 June 2024. (d) Row sums of matrix AVK from CrIS. (e) Similar to (b), but for GIIRS, CrIS, and GEOS-CF without interpolating. For GIIRS, retrievals are performed below 200 hPa, and a single a priori profile is applied to all observations, in which the lowest layer is adjusted by interpolating to the surface pressure obtained from ERA5.

Figure S4: the titles of panels do not seem to match the caption. Please double check.

Response: Thanks for pointing this out. This figure has been updated to Fig. S5. We have carefully checked this figure and revised both the panel titles and the figure caption to ensure that each title accurately corresponds to the description in the caption.

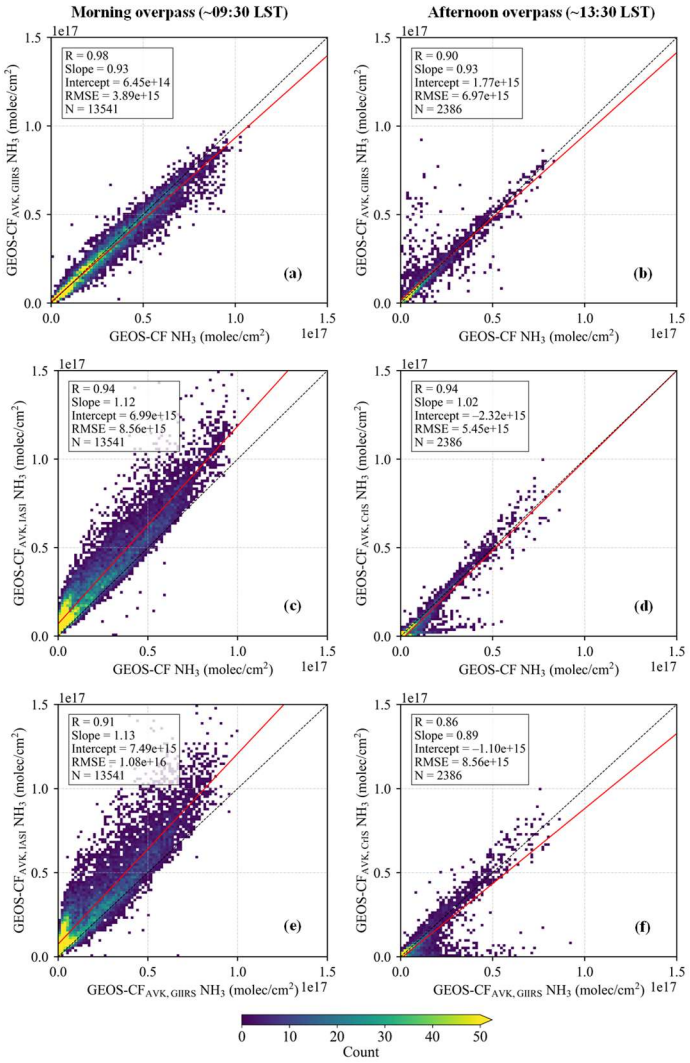

Figure S4. Comparison of the modelled NH_3 columns over the North-Northeast China Plains (30°–43°N, 110°–125°E) in June 2024, derived from GEOS-CF model profiles with satellite AVKs smoothing. Data pairs

correspond to the same grid cells and overpass times. Panels (a) and (c) are comparisons of modelled NH_3 columns at morning overpass times after AVK smoothing for GIIRS and IASI, respectively, relative to the original total column values. Panels (b) and (d) are similar comparisons at afternoon overpass times for GIIRS and CrIS, respectively. Panels (e) and (f) show cross-comparisons between modelled NH_3 columns smoothed using different satellite AVKs: (e) GIIRS vs. IASI, and (f) GIIRS vs. CrIS.

Figure S8: are the green dots all GIIRS observations? Please clarify in the caption.

Response: Thanks for your suggestion. This figure has been updated to Fig. S9. The green points in the figure indeed correspond to GIIRS NH_3 observations. Because FY-4B/GIIRS is a geostationary satellite, its observations are acquired at largely fixed locations, resulting in repeated measurements at the same positions. In the revised manuscript, the figure caption has been updated to provide a more detailed description.

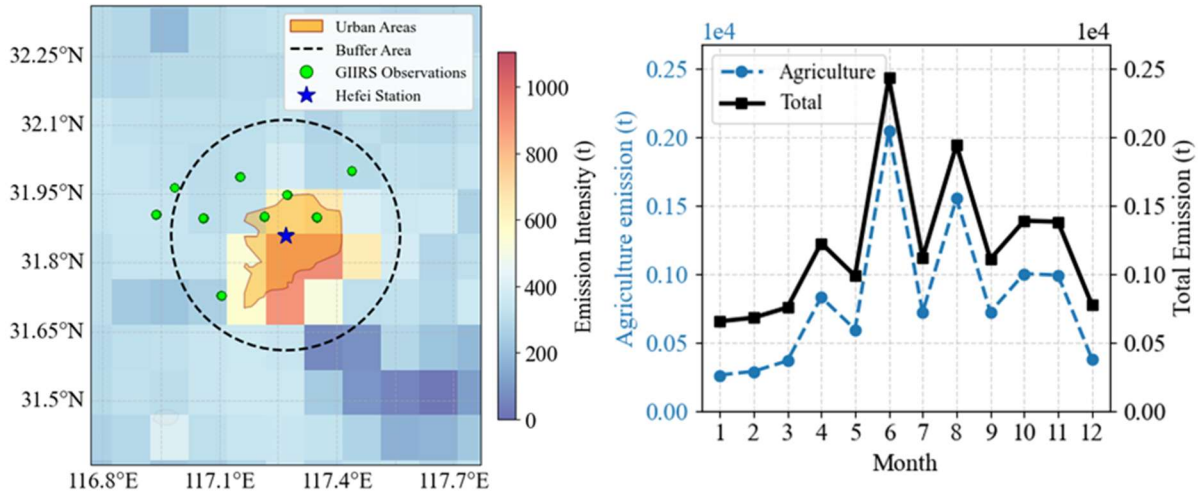

Figure S5. Spatial and temporal pattern of ammonia emissions in 2017 from the MIX emission inventory at the Hefei station. (a) Spatial distribution of anthropogenic NH_3 emissions and GIIRS observations. The green points represent locations where GIIRS observations were repeatedly acquired and the corresponding NH_3 retrievals satisfied the filtering criteria applied in this study. (b) Monthly timeseries of anthropogenic NH_3 emissions. The blue stars indicate the locations of Hefei station (31.91°N, 117.17°E), as described in Sect. 3.2.

Figure S11: please provide the spatial coverage.

Response: Thanks for your comment and suggestion. This Figure has been updated to Fig. S13. It shows the temporal variations of GIIRS-derived NH_3 columns and the corresponding statistics within a 0.25° latitude/longitude radius around the Hefei station, including retrieval errors, thermal contrast (TC), and the bottom layer of column averaging kernels (AVKs). In the revised manuscript, the figure caption has been supplemented to clarify the spatial coverage of the observations.

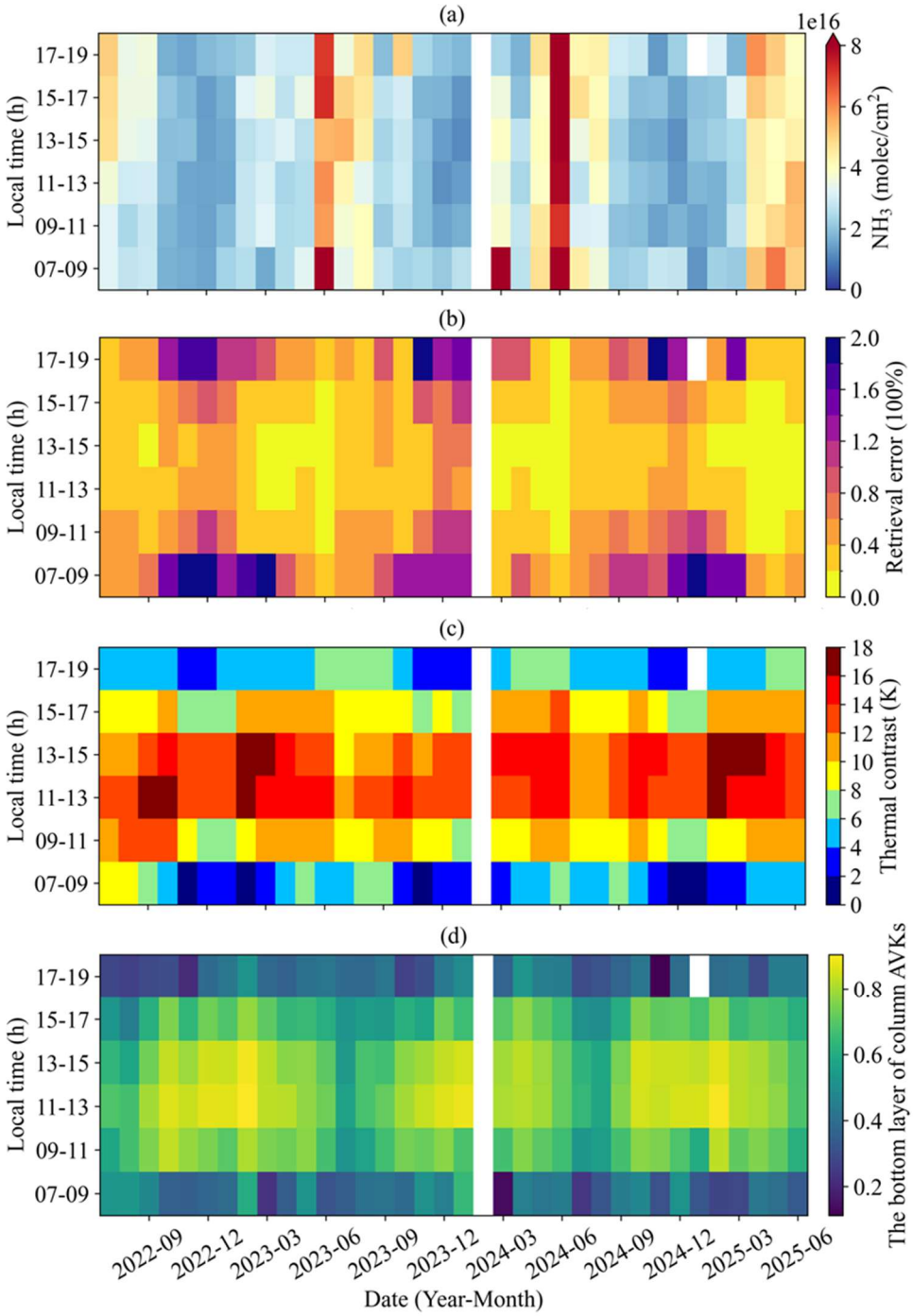

Figure S6. Temporal variations of (a) NH_3 columns, (b) the corresponding retrieval error, (c) TC, and (d) the bottom layer of column AVKs. These statistics are calculated from FY-4B/GIIRS NH_3 retrievals within a 0.25° latitude/longitude radius around the Hefei station.